*Article*

# Muscle Activation–Deformation Correlation in Dynamic Arm Movements

**Bangyu Lan *** and **Kenan Niu**

Robotics and Mechatronics Group, The Faculty of EEMCS, University of Twente,
P.O. Box 217, 7500 AE Enschede, The Netherlands; k.niu@utwente.nl
* Correspondence: b.lan@utwente.nl

**Abstract:** Understanding the relationship between muscle activation and deformation is essential for analyzing arm movement dynamics in both daily activities and clinical settings. Accurate characterization of this relationship impacts rehabilitation strategies, prosthetic development, and athletic training by providing deeper insights into muscle functions. However, direct analysis of raw neuromuscular and biomechanical signals remains limited due to their complex interplay. Traditional research implicitly applied this relationship without exploring the intricacies of the muscle behavior. In contrast, in this study, we explored the relationship between neuromuscular and biomechanical signals via a motion classification task based on a proposed deep learning approach, which was designed to classify arm motions separately using muscle activation patterns from surface electromyography (sEMG) and muscle thickness deformation measured by A-mode ultrasound. The classification results were directly compared through the chi-square analysis. In our experiment, six participants performed a specified arm lifting motion, creating a general motion dataset for the study. Our findings investigated the correlation between muscle activation and deformation patterns, offering special insights into muscle contraction dynamics, and potentially enhancing applications in rehabilitation and prosthetics in the future.

**Keywords:** arm movements; sEMG; A-mode ultrasound; muscle contraction dynamics; muscle activation; muscle deformation

## 1. Introduction

In daily activities, we use our arms to complete various motor tasks. When arms are raised to act, arm muscles thus activate, generating motor unit action potentials (MUAPs) that are typically associated with certain levels of muscle deformation [1–3]. This muscle contraction dynamics involves a correlation between muscle deformation and activation, which is essential for various daily activities. For example, patients with fasciculohumeral dystrophy (FSHD) exhibit reduced muscle strength and altered contraction dynamics [4]. Detecting changes in the muscle activation–deformation pattern can enable early diagnosis and timely treatment.

Similarly, recognizing muscle contraction dynamics (the correlation between muscle activation and deformation) is critical in robotic prosthesis control, as it helps optimize the system for more intuitive and natural user interactions [5,6]. In athletic training, monitoring the correlation between muscle characteristics enables the optimization of movements and postures [7], thereby improving performance and reducing injury risk. Furthermore, therapeutic protocols can benefit from balanced muscle activation and deformation, which helps prevent muscle under-stimulation or overexertion [8].

To deepen the understanding of this relationship between muscle activation (induced by neuroelectrical signals) and the associated muscle deformation (representing the biomechanical signal), and also gain insight into the dynamics of the interaction, researchers have used torque, force, or motion classification as prediction targets from muscle activation or deformation signals and then applied these predictions to address real-world challenges. For example, the differences in muscle contraction onset detected by ultrasound and electromyography could be used to assess neuromuscular control and joint stability [9]. Ref. [10] compared the efficacy of gesture classification and muscle contraction force estimation from ultrasound and sEMG independently, and later combined the two modalities for enhanced task performance [11]. Similarly, Ref. [12] evaluated the performance of analyzing muscle fatigue from muscle activation and deformation, while [13] examined the identification of muscle fasciculation. Although these studies worked on the application of the relationship between muscle deformation and activation, there was limited research directly exploring this relationship using only raw neuromuscular signals and original muscle deformation data to provide more compelling evidence.

Therefore, an alternative approach to exploring this relationship is directly investigating the correlation between muscle activation and deformation. Signals generated by muscle activation (in the form of MUAPs) can be captured directly through sEMG devices [14]. In contrast, muscle deformation, as a mechanical parameter, is normally measured by the ultrasound device [15,16]. Among various ultrasound techniques, Amplitude mode (A-mode) has demonstrated good accuracies for biometric depth measurement [17,18]. To investigate the relationship between signals measured by the two devices (sEMG and ultrasound) is important, as these signals are the intact biological signals generated by the human body. This relationship may provide an important basis for the exploration of muscle contraction dynamics at a higher level.

In summary, this study aimed to compare the classification results of the motion types separately from sEMG signals (muscle activation patterns) and ultrasound signals (muscle thickness deformation), which is beneficial to understanding the correlations between two muscle features. This comparison is critical because many studies rely on this relationship for various functional muscle applications, such as assessing muscle fatigue, performing functional muscle analysis, or diagnosing muscle diseases (such as FSHD [4]). By establishing this comparison, this work could be beneficial in establishing qualitative or even quantitative correlations to relate muscle deformation and activation in the future.

## 2. Materials and Methods

In this section, the devices used and the designed experiments are described for collecting the required datasets. After that, the details and rationale of the proposed attention UNets are illustrated, together with the evaluation methods, which analyze the correlations between muscle activation and deformation.

### 2.1. Overview of the Study

The overview of this study is illustrated in Figure 1. To collect the muscle activity dataset, six healthy participants were invited to perform specific movements. Each participant wore an sEMG device and an A-mode ultrasound transducer on their arm while performing the specified arm movement. A stereo camera was positioned in front of the participants to record the trajectory of the moving arm. During the experiment, a repeatable continuous movement of lowering and lifting the arm was recorded.
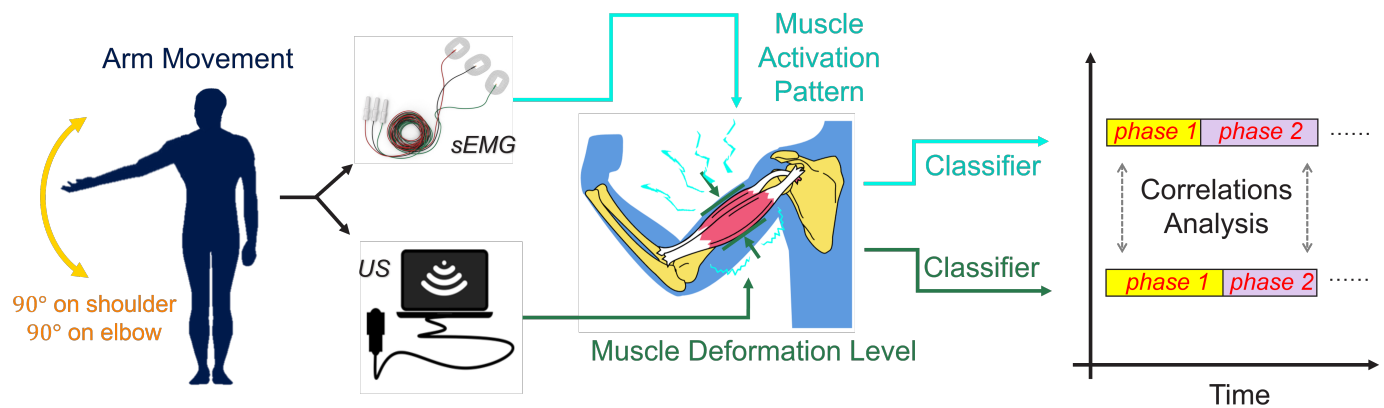
**Figure 1.** The overview of this study for exploring the relationship between muscle activation and deformation. Several participants were invited to join the arm movement experiment and the recorded sEMG and A-mode ultrasound signals were collected. The joint angles were also recorded via an additional stereo camera (not displayed here). The arm motions were divided into two phases (lifting and putting down the arm), and the models were trained to classify motion phases from the separate recorded signals. The correlation between the two classifications was analyzed.

After the experiment, the synchronized sEMG and ultrasound signals were pre-processed and fed into two separate networks to segment the motion phases. The motion phases were labeled on the basis of changes in joint angles corresponding to the lifting or lowering of the arm. The models were trained to learn the correlations between muscle features and the phases of joint angle changes. Initially, a dataset from five participants was used to train the model to capture general muscle-motion phase mappings. Subsequently, the model was fine-tuned using a small portion (20%) of the data from the sixth participant to adjust for individual muscle characteristics. Finally, the learned mappings were evaluated using the remaining 80% of data from the same participant. This approach ensured that the network learned the muscle characteristics (activation or deformation) rather than overfitting the data of a specific participant.

During evaluation, in addition to analyzing the classification accuracy, the classifications derived from the two signals were statistically compared to assess their correlation. This analysis validated whether the muscle activation and deformation patterns were significantly correlated.

## 2.2. Human-Related Experiments

### 2.2.1. Participant Recruitment Strategy

In this experiment, six participants were recruited to produce sEMG and ultrasound datasets. The participants were mainly graduate students (aged 20–30) from our Robotics and Mechatronics research group. The recruitment process was totally random and based on personal willingness. However, participants could not have a history of arm injuries or discomfort. Also, due to the limitations of measurement devices, overweight or strong persons had been excluded due to the potential over-thick or fatty arms which were difficult for the measurement. The collected datasets were used to validate if the correlations between two types of neuromuscular features indeed existed. This human-related experiment was approved by the Ethics Committee of Information & Computer Science at the University of Twente (Application No. 240688). Each participant was informed of the experimental details from the informed consent form before the experiments.

### 2.2.2. EMG Preparation and Setup

The sEMG device used in this study is shown in Figure 2. It consisted of a custom-designed, 3D-printed system with eight channels of dry electrodes and a custom-developed amplifier [19]. Among the eight channels, three electrodes were attached to the biceps brachii and another three to the triceps brachii. These six electrodes, each with a diameter of 20 mm, were fabricated from PI-ETPU 85-700+ (Palmiga Innovations, Jonstorp, Sweden) and connected to the amplifier via CI-1036 stretchable silver-ink (Engineered Conductive Material, Delaware, OH, USA). Each set of three electrodes was arranged in a triangular configuration and integrated into a stretchable fabric band 3D-printed with X60 Ultra-Flexible Filament. The remaining two electrodes served as references for average and ground-level voltage measurements. Signal amplification was achieved using an ADS1298 analog front-end IC from Texas Instruments, with common-mode and differential input impedances of approximately 1.5 G$\Omega$ and 0.5 G$\Omega$ at 50 Hz. Raw signals were recorded without filtering to preserve subtle features that might correlate with motion cycles or muscle deformation.
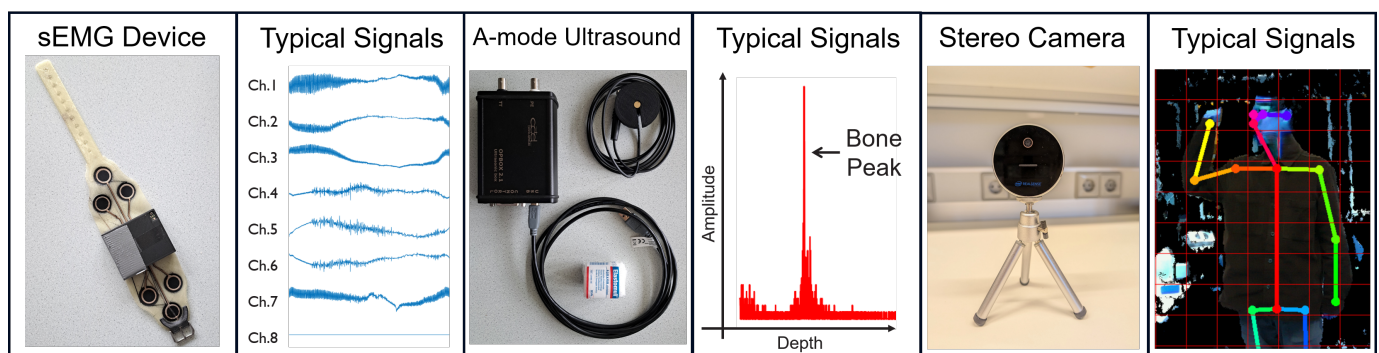


**Figure 2.** Three devices used in this study and their typical signals. The sEMG recorded muscle activation patterns. The A-mode ultrasound recorded the bone movements, which later were transformed to muscle deformation. The stereo camera recorded the RGBD images first (the image had been blurred and processed for privacy issues), then recognized the 3D joint movements through an algorithm, and calculated the joint angle from the joint positions in the end.

To ensure proper attachment and signal quality, participants rested in a cool environment for 5 min before electrode placement to allow any sweat on the skin to evaporate, ensuring a dry surface. The skin areas where the electrodes were placed were then thoroughly cleaned to remove dirt and oil, ensuring optimal signal quality. Cleaning was performed using alcohol wipes, which effectively removed the oils and debris. The muscle bellies of the biceps brachii and triceps brachii on the right upper arm were visually identified based on the participants' arm movements. Three electrodes were carefully placed on the belly of the biceps brachii and another three on the belly of the triceps brachii, with the amplifier box oriented toward the wireless receiver to optimize signal transmission. A stretchable fabric band was used to firmly secure the electrodes. Before the experiment, participants were asked to wave their arms repeatedly while monitoring the sEMG signals to confirm consistent patterns and ensure reliable signal acquisition.

### 2.2.3. Ultrasound Preparation and Setup

The A-mode ultrasound device was the OPBOX version 2.1 (OPTEL Ultrasonic Technology, Wrocław, Poland). The device was set to 100 MHz sampling frequency, 4 to 25 MHz bandwidth analog filters, +30 dB constant gain, and +24 dB pre-amplifier to increase the peak visibility of raw signals. The x-axis (distance) of ultrasound signals had been shifted a personalized amount of time to only focus on the area where the bone peaks most likely

appeared. This was determined in the following way: For each participant, the recorded A-mode ultrasound signals were compared with the B-mode ultrasound images to find the approximate range of muscle contraction, i.e., where the bone peak mostly existed (see Figure 3, demonstrated by examples of two participants). As most tissues between the bone and the skin were skeletal muscles [20], we treated this distance as the approximated muscle thickness. The technique using ultrasound to track the bone positions and movement followed [16,21–24].
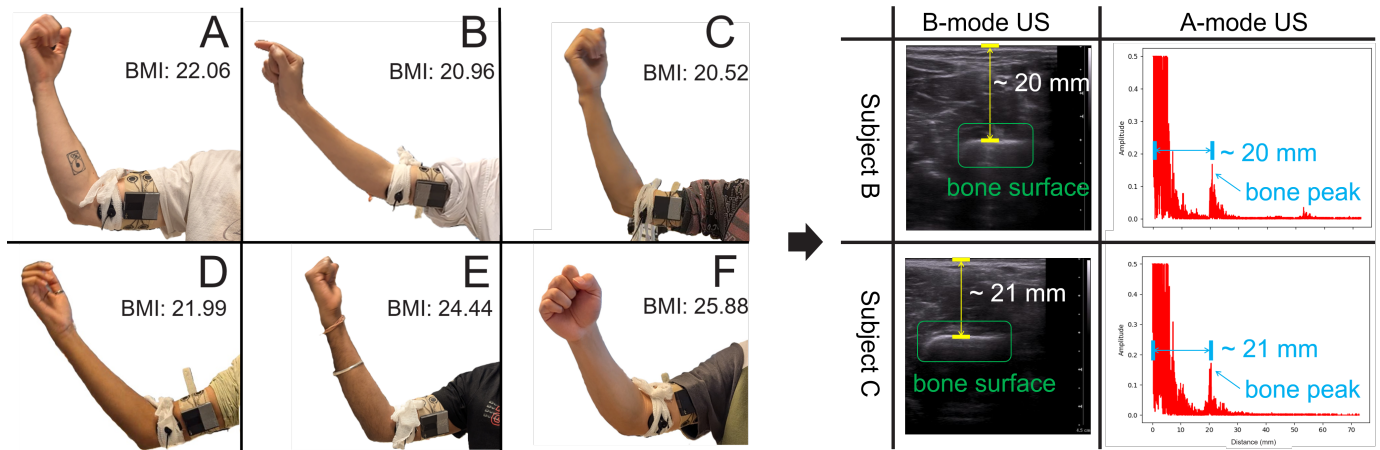


**Figure 3.** The preparation of each participant's experiment. Six different participants (**A**–**F**) were invited to wear the sEMG device and A-mode ultrasound. The positions of the devices were first put on the approximate positions, then were adjusted to check the clear pattern locations. The right figure demonstrates how we validated the bone peak positions in A-mode signals, using the example from Participant B and Participant C.

2.2.4. Stereo Camera Preparation and Joint Movement Recording

The stereo camera was a LiDAR camera (L515 product from Realsense series, Intel, Mountain View, CA, USA). It specifically uses time-of-flight (ToF) technology to calculate the 3D space distance, which inherently avoids the need for geometric calibration typically required in the systems with two monocular cameras. As the L515 generated both point clouds and RGB images simultaneously using ToF, additional camera calibration was not performed.

To track the arm movement positions from a camera, we first obtained the RGB videos from the camera, then recognized the joint positions through the OpenPose algorithm ([25]). This is demonstrated in the right side of Figure 2. The OpenPose algorithm has been used in many previous studies for identifying 3D joint movements [26–28]. As the RGB images corresponded to the depth images for each pixel, we directly extracted 3D coordinates from the depth images. The changes in these coordinates were used as the 3D positions of the arm movements. After knowing the 3D positions of arms, joint angles could be further calculated through the cosine theory in the 3D space [29–31]. This was achieved via Equation (1):

$$\cos\theta = \frac{\mathbf{v}_1 \cdot \mathbf{v}_2}{\|\mathbf{v}_1\|\|\mathbf{v}_2\|} \tag{1}$$

while the limb vectors $\mathbf{v}_1$ and $\mathbf{v}_2$ were calculated as follows. The $\mathbf{p}_{shoulder}$, $\mathbf{p}_{elbow}$, and $\mathbf{p}_{wrist}$ represent the 3D positions of shoulder, elbow, and wrist of the participant.

$$\mathbf{v}_1 = \mathbf{p}_{elbow} - \mathbf{p}_{shoulder}$$
$$\mathbf{v}_2 = \mathbf{p}_{wrist} - \mathbf{p}_{elbow} \tag{2}$$

### 2.2.5. Summary of Devices Setup and Movement Description

Before the arm movement experiment started, the participants wore the sEMG device on the right upper arm and attached an A-mode ultrasound transducer around the right elbow. The placement of the A-mode ultrasound and sEMG devices is illustrated in Figure 3. At these positions, A-mode ultrasound provided clear bone peaks in the recorded signals, which had been confirmed using the B-mode ultrasound. These bone peak movements were interpreted as indicators of muscle mechanical deformation. The sEMG device placement enabled precise recording of bicep and tricep muscle activation. Additionally, with the Octopus device oriented towards the laptop, Bluetooth communication was stable, ensuring uninterrupted signal transmission. During the experiments, participants did not report any discomfort or issues related to wearing the ultrasound or sEMG devices.

In the front of participants, the stereo camera was put on a high platform to track the movements. The participants stood at a place where the stereo camera could capture the whole upper body via video streams, which made it easy for OpenPose to recognize the movement of the right arm. The whole setup is on the left side of Figure 4. During the experiment, the participants performed the defined motion cycle illustrated on the right side of Figure 4. The participants lifted their right arm from the downside to above the shoulder, then bent the elbow so that the fist could towards the head (motion phase 1). After that, the participants returned the arms gradually to their original positions (motion phase 2). The full motion cycle (phases 1 and 2) lasted for around six to nine seconds. This time varied both between different participants and between different motion cycles of the same participant. The whole recording lasted for five minutes. This motion of raising the arm focused on shoulder and elbow movements that are commonly seen in daily tasks (e.g., lifting, reaching, or manipulating objects overhead). It involves abduction/adduction of the glenohumeral joint and flexion/extension of the elbow. Thus, it can partially represent the arm movements in daily activities.
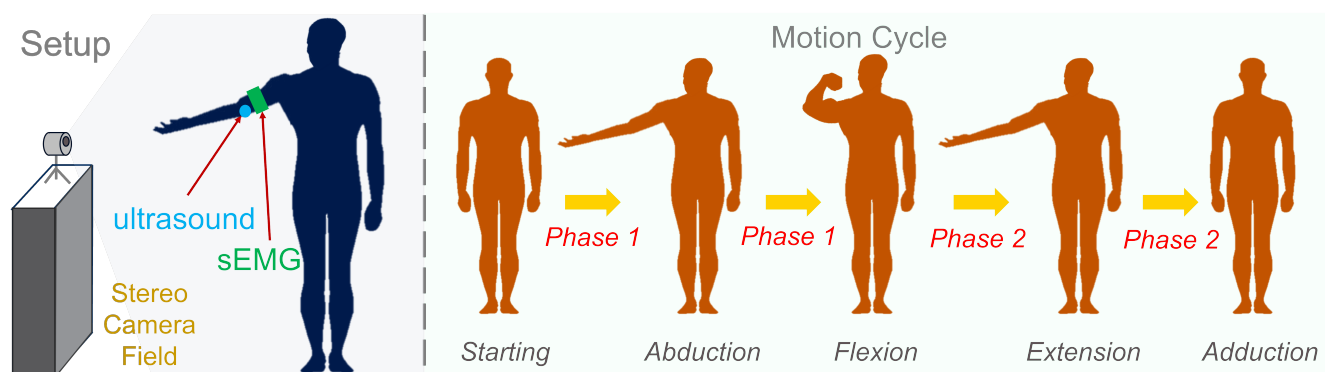


**Figure 4.** The experiment's setup and the specified movement of participants. In the left figure, the relative positions between the three devices are demonstrated, together with the participant's position. In the right figure, the participant's specified movement and the motion phases are demonstrated.

Noticed that since there was no requirement for the exact positions that the arm movement should reach, the participant's arm could move to any position (towards the head) freely in different motion cycles. Thus, this dataset could evaluate the correlations between muscle activation and deformation even when they had large variance patterns within a single participant's movement.

### 2.3. Signal Processing

For the signals recorded in the experiments, the sEMG signals were sampled at 1000 Hz, the A-mode ultrasound was run at 30 Hz, and the arm tracking algorithm was at

10 Hz. After experiments, the signals of all devices were collected and pre-processed for effective network training.

For each channel of sEMG signals, the amplitude was normalized to range (0, 1) to improve the visibility of tiny features. For A-mode ultrasound, peak detection was used in the bone peak appearance range to find the highest peak movement [16,21–24,32]. The trajectory of the bone peak movement was used as the muscle thickness deformation. This trajectory was smoothed to remove the outliers (recognized as the points that are out of the [5%, 95%] distribution range of bone peak positions), then was also normalized to the (0, 1) range as the input of networks. For the recorded arm movement positions, the outliers were removed first and the data were smoothed using the moving average [33] to remove the noise. After that, the joint angles were calculated. Depending on the changing patterns of the angle (either becoming smaller or larger), the continuous motions were segmented into two phases (Figure 4), being the training targets.

To address the varying sampling rates of recorded signals, data synchronization was performed. To achieve this, timestamps were simultaneously recorded for each sensor during the experiments, and the 30 Hz from ultrasound was set as the standard alignment sampling rate. For arm tracking data, the missing 3D joint positions (due to the discrepancy between 10 Hz and 30 Hz) were interpolated via quadratic functions [34,35], with the assumption of continuous arm motion. For the sEMG signals, any additional data points not aligned with the ultrasound timestamps were discarded; only the samples closest to the ultrasound timestamps were kept. In the end, the synchronized data streams from each participant were used for training and evaluating the proposed attention UNets model.

### 2.4. Deep Learning Methodology

2.4.1. Network Training Tasks

We established two training tasks to facilitate the comparison of classification results between the two types of bio-signals. The first task involved classifying the type of motion transition. When feeding signals into the networks, a transition vector was included to indicate the starting position of a new motion cycle. However, whether the onset referred to a transition from arm lifting to lowering (increasing angles) or the reverse (decreasing angles) was unknown. The network needed to classify this onset transition of a motion cycle based on the full cycle of bio-signals. By comparing the transition classifications from both sEMG and ultrasound signals, we assessed their correlations between muscle activation and deformation.

The second task (motion phase segmentation) focused on comparing the full sequence motion classification between the two muscle signals. During different motion phases, muscle activation and deformation may display unique yet consistent patterns. The classification of these patterns could determine whether the muscle features captured by the two signals were correlated at each corresponding moment. Additionally, by analyzing the classification positions in the two signals, we could identify any other special patterns of each muscle feature.

2.4.2. Network Structure

As our targets involved segmenting motion phases using the original bio-signals, we chose a classical UNet model (Figure 5) inspired by [32,36,37]: this model produced an additional transition classification from the encoder in addition to the continuous motion segmentation. We designed the networks for two objectives: (1) to see if the motion classifications were similar for the two signals over the full sequence and (2) to compare the motion transition classification of the two signals at the onset of a new motion cycle. This structure was used for both ultrasound signals and sEMG signals for fairness. For each

modified attention UNet, the structure consisted of a five-layer encoder and decoder, which were directly connected and shared information through the skip-connections in the same layer. The encoder provided the classification for the transition at the beginning of this period, while the decoder outputted the classification for each moment of the signals.
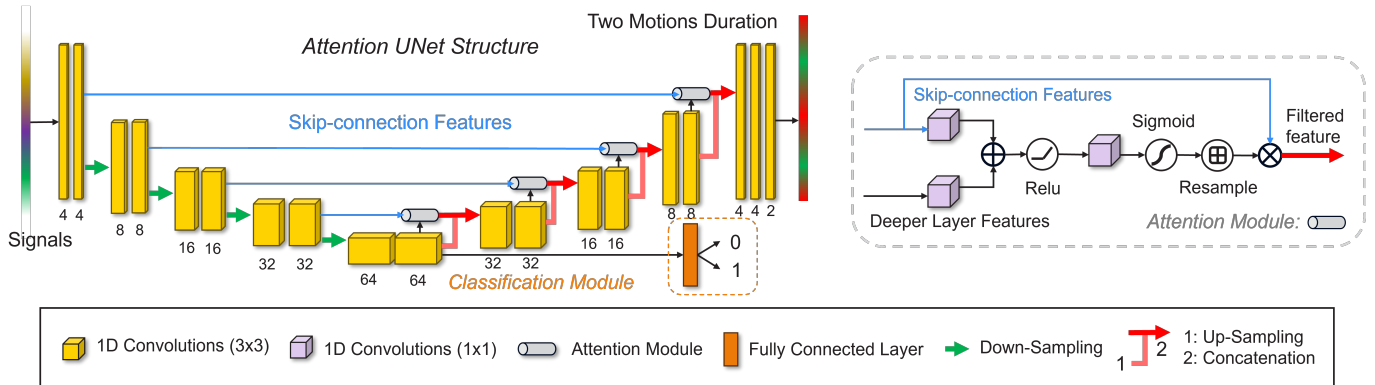


**Figure 5.** The proposed attention UNet for predicting the arm movement phase using ultrasound signals. The input is the recorded bio-signals, while the output from the encoder is the classification of movement transitions, and the final output is the motion types throughout the full sequence (red and green represent the two motion phases). The attention module has a horizontal cylindrical shape and is demonstrated on the right in detail.

In Figure 5, each convolution (yellow) block in the main attention UNet consists of 1D convolution, batch normalization, and an ELU activation function [38]. The down-sampling used the max-pooling in one dimension, while the up-sampling used the nearest neighbor interpolation.

### 2.4.3. Training Strategy

To train the proposed neural network to identify correlations between bio-signals and joint angles, three training losses were designed: two classification losses, $l_{trans}$ and $l_{phase}$, and one dice loss, $l_{DL}$. These losses enable the network to learn onset transition classification and full motion sequence classification effectively.

For the transition classification and full motion sequence classification, we used the cross-entropy losses $l_{trans}$ and $l_{phase}$, respectively. As $l_{phase}$ was applied on each point of the input sequence, it was a segmentation problem, where the dice loss $l_{DL}$ was also used as Equation (3). The $p_i^{pred}$ and $p_i^{true}$ were the prediction probability and the ground truth label at this moment, $n$ was the number of all moments in this sample, and $\epsilon$ ensured the numerical stability during training. The dice loss calculated the dice coefficients of segmentation and transformed it as a loss function to enable networks to have largeroverlapping areas between the segmentation and the ground truth. In the end, the total loss function was written as Equation (4).

$$l_{DL} = 1 - \frac{2\sum_{i=0}^{n}(p_i^{pred} * p_i^{true}) + \epsilon}{\sum_{i=0}^{n} p_i^{pred} + \sum_{i=0}^{n} p_i^{true} + \epsilon} \tag{3}$$

$$l = l_{trans} + l_{phase} + l_{DL} \tag{4}$$

To validate whether the networks could learn general mappings between bio-signals and motion phases, rather than overfitting to a specific case, we designed a two-stage training process. First, the network was pre-trained using a dataset from five participants to capture generalizable patterns. Then, the model was fine-tuned using a small percentage (20%) of data from another participant and evaluated on the remaining 80% of that participant's dataset. This approach ensured that the learned mappings were generalizable while

allowing the model to adapt to individual variations in muscle deformation and activation patterns with minimal additional data.

During training, we used a 0.0001 learning rate, with the Adam optimization method [39]. The pre-training stage lasted for 50 epochs, while the fine-tuning stage lasted for another 30 epochs. Then, we selected the epoch result of the two models from the 30 epochs when they had closed classification accuracy.

*2.5. Statistical Analysis and Evaluation*

2.5.1. Chi-Square Test

To evaluate and demonstrate the correlations between muscle activation and deformation, we compared the classification results from sEMG and ultrasound signals using statistical analysis. Specifically, the chi-square test was employed to determine whether a significant relationship existed between the predictions made by the two models. The purpose of the test was to assess if the observed agreement between the two models' classification results could be attributed to a true relationship between muscle activation and deformation patterns, rather than occurring by chance.

The chi-square test is a statistical method used to compare observed results (from the two models) with expected results (assuming no correlation between the models' classifications). Its goal is to determine if differences between the observed and expected values indicate a genuine relationship between the variables being studied—in this case, the classification outputs from sEMG and ultrasound signals. This approach allowed us to evaluate the statistical significance of the correlation between the two signals.

Three assumptions of the chi-square test were fulfilled. (1) Independence of observations: each classification decision was made independently by either the sEMG or ultrasound model. (2) Adequate expected frequencies: the contingency table of classification decisions was verified to ensure that all expected frequencies were greater than 5, following the threshold defined in [40]. (3) Categorical data: this assumption was inherently satisfied, as the task involved two classification categories. The chi-square statistic ($\chi^2$) was calculated using Equation (5):

$$\chi^2 = \sum \frac{(O_{ij} - E_{ij})^2}{E_{ij}} \tag{5}$$

The $O_{ij}$ is the observation, while the $E_{ij}$ is the expected frequency. The chi-square test used the $\alpha = 0.05$ as a standard to reject the null hypothesis, which suggested the existence of the correlations between two sequences of decisions. This was performed to analyze the decision correlations between ultrasound and EMG signals from each participant.

2.5.2. F1-Score

To evaluate the similarity between the transition classification of the two models, we used the F1-score as a metric. Unlike the traditional use of the F1-score to assess the agreement between predictions and ground truth, in this study, the F1-score was computed between the binary prediction outputs of two models. This evaluation aimed to measure the level of agreement and similarity between the two models' transition classification behaviors.

The F1-score was derived from the harmonic mean of precision and recall, which were defined based on the confusion matrix elements calculated between the results from ultrasound and sEMG models. During testing, unlike the training setup (mentioned in Section 2.4.1 Network Training Tasks), the full period transition was set as lowering the arm to lifting the arm, and the model needs to correctly classify that a new period starts from lifting the arm. Thus, lifting the arm was set as the positive while the lowering the arm was set as the negative answer. The confusion matrix was defined as follows:

- True Positives (TP): Transitions where both models classified the starting motion as lifting the arm.
- False Positives (FP): Transitions where ultrasound model classified the motion as lifting the arm, but sEMG model classified as lowering the arm.
- False Negatives (FN): Transitions where ultrasound model classified the motion as lowering the arm, but sEMG model classified as lifting the arm.
- True Negatives (TN): Transitions where both models classified the starting motion as lowering the arm.

Based on these elements, the precision and recall were calculated as follows:

$$\text{Precision} = \frac{\text{TP}}{\text{TP} + \text{FP}}$$

$$\text{Recall} = \frac{\text{TP}}{\text{TP} + \text{FN}}$$

The F1-score was then given by the harmonic mean of precision and recall:

$$\text{F1-Score} = 2 \times \frac{\text{Precision} \times \text{Recall}}{\text{Precision} + \text{Recall}} \tag{6}$$

In this context, the F1-score quantified the similarity between the transition classification of the two models, focusing on their agreement for the correct motion classification when a new period started. A high F1-score indicated strong alignment in their classifications, suggesting similar correct decision-making patterns. Conversely, a low F1-score reflected discrepancies in their classifications.

### 2.5.3. Other Evaluation Metrics

Before analyzing the correlation and performing the chi-square test, the classification accuracy, Acc(%) in Table 1, was calculated for both sequence and transition classification tasks using the ultrasound (US) and sEMG models. Classification accuracy was defined as the alignment between the model's predictions and the ground truth labels in percentage.

**Table 1.** The table used to compare the classifications from both the ultrasound (US) and sEMG models. The sequence classification means the classification of motion types for each moment during the whole sequence, while the transition classification means the classification of the transition type for the start of each motion cycle. Acc(%) represents the classification accuracy of the whole sequence from each model compared with the ground truth labels. Correlation(%) represents the same classification decision made from the two models, regardless of the accuracy. The *p*-value is from the chi-square test to validate if there is a significant relationship between the classification results from the two models.

| Participant | Sequence Classification Comparison | | | Transition Classification Comparison | | |
|---|---|---|---|---|---|---|
| | US/EMG Acc (%) | Correlation (%) | *p*-Value | US/EMG Acc (%) | Correlation (%) | F1-Score (%) |
| A | 96.62/85.03 | 85.55 | 0.0000 | 100.0/93.10 | 93.10 | 96.43 |
| B | 73.40/72.46 | 64.26 | 0.0000 | 70.59/41.18 | 70.59 | 73.68 |
| C | 89.76/92.61 | 91.97 | 0.0000 | 90.91/81.82 | 84.85 | 91.23 |
| D | 92.56/49.04 | 52.63 | 0.0279 | 100.0/23.53 | 23.53 | 38.10 |
| E | 85.62/58.16 | 57.22 | 0.0000 | 100.0/67.65 | 67.65 | 80.70 |
| F | 88.70/61.70 | 64.00 | 0.0000 | 93.94/57.58 | 57.58 | 72.00 |

For the sequence classification task, the ground truth corresponds to the motion type at each moment (see Figure 6 for the classification of the full sequence). For transition

classification, the ground truth refers to the starting motion type of a new motion cycle, which the models needed to predict using the output of the classification module shown in Figure 5.
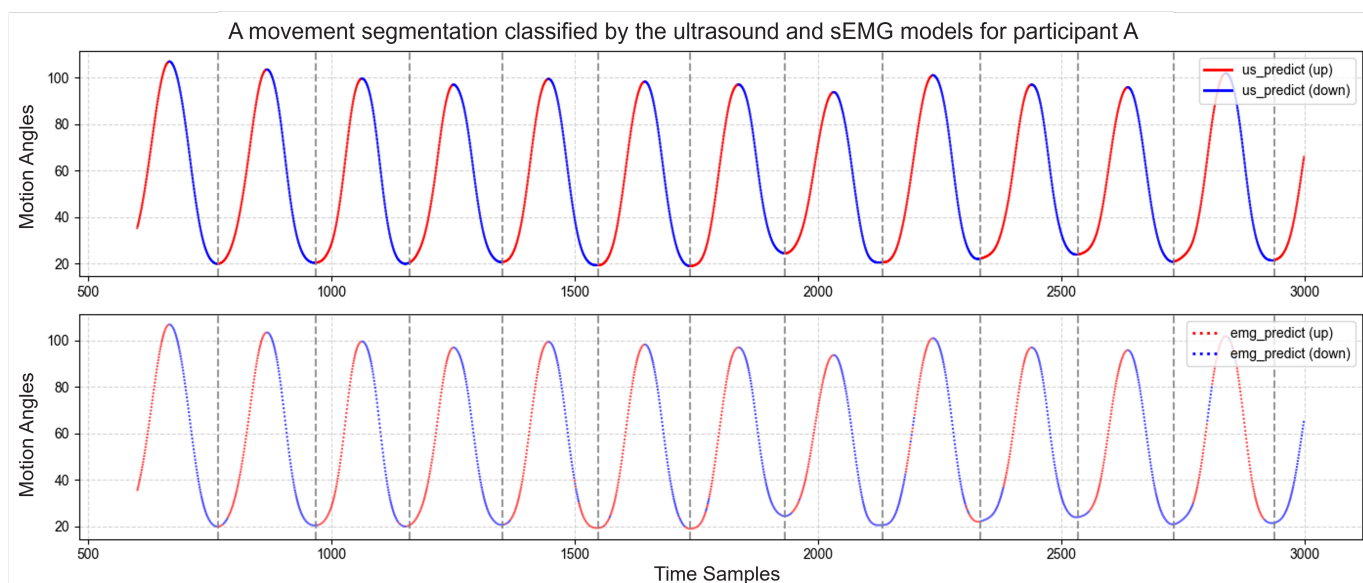


**Figure 6.** This shows the classification results from the two models of participant A. A random segment of the motion cycles was selected from the test dataset, which contains several motion cycles (due to the repeatable motion). The solid curves represent the prediction results from the ultrasound model, while the dotted curves represent the results from the EMG model. The red color represents the class of lowering the arm, while the blue color represents the class of lifting the arm. The gray vertical dashed lines represent the prediction positions from the ultrasound model.

In addition, another metric (the Correlation(%) in Table 1) was reported as a descriptive metric of agreement during the analysis. It calculated the proportion of matching classification decisions between the ultrasound and sEMG models. However, to assess the statistical significance of this observed agreement quantitatively and provide a more rigorous analysis, the chi-square test was conducted as the primary method for the statistical analysis.

## 3. Experimental Results

### 3.1. Evaluation Objectives

After training the model, the inference results from the two models (ultrasound and sEMG) and the ground truth labels in the test dataset were analyzed to explore the relationship between muscle activation and deformation. In addition to evaluating the classification accuracy, the classifications from the two models were compared to assess their agreement. The chi-square test was employed to determine whether the observed agreement between the classifications of the ultrasound and sEMG models was statistically significant, providing evidence of a potential relationship between muscle activation and deformation. Specifically, the test assessed whether the observed frequencies of agreement and disagreement differed significantly from what would be expected under the null hypothesis (i.e., no relationship between the classifications).

### 3.2. Evaluation Results

To explore the correlations of classification from the ultrasound and sEMG signals, the classification results are reported on the left side of Table 1. The accuracy Acc% (and all the subsequently mentioned "accuracy") refers to the classification accuracy of the model, which is determined by comparing it with the ground truth labels of the full

motion sequence. For all participants, the *p*-values calculated using the chi-square test are lower than 0.05, rejecting the null hypothesis that there is no correlation between the two classification sequences. The third column Correlation(%) refers to the percentage of the same classification decisions made from the ultrasound and sEMG models. Notice that although for participants D, E, and F, the sEMG model prediction accuracies were quite low, the Correlation(%) values are still very close to (or even higher than) the EMG prediction accuracies. Also the *p*-values that were close to zero demonstrate the clear significant relation between the two signals. This demonstrates that between muscle activation and deformation there exists a clear relationship, even when the sEMG model did not perform well for some cases.

Another result is the transition classification performance, shown in the right side of Table 1. During the evaluation, the onset transition vector given to the network was from putting down to lifting up the arm. In this way, the model knew that a new motion cycle started and tried to classify the transition position (from lifting up to putting down the arm) within a single motion cycle (see Figure 6). The transition positions determined from the ground truth labels were used to calculate the F1-score, which evaluated the performance of the two models. The comparison of their transition classifications at these specific positions was reported in the last column of Table 1. Except for participant D, other participants obtained very high F1-scores, showing that the two models have similar classification results on the onset transition positions.

To evaluate the models' capability to locate the transition positions, a qualitative comparison result of the motion classification was visualized in Figure 6. This is from a random segment of the continuous motion performance of participant A. Figure 6 shows (1) the full sequence classification results for both the ultrasound and sEMG models and (2) the predicted transition positions in the ultrasound model, demonstrated by the vertical dashed gray lines.

In addition to the classification accuracy, the direct comparison between the two models' classifications is visually shown in the contingency tables from Figure 7, which helps to explore any potential relationship between muscle activation and deformation. Without comparison to the ground truth labels, these tables intuitively illustrate the correlations between the classification decisions from the two models.

In Figure 7, the first row shows the relationship between the decisions of the two models for participants A, B, and C. These three tables show strong correlations, as the predominant values are along the diagonal of the table, indicating a high level of agreement. In contrast, the second row, representing the models' classifications from the participants D, E, and F, shows lower correlations, as the frequency of the disagreements equals to or exceeds that of agreements.

Furthermore, since the motion classification was performed point-by-point across the entire signal sequence, the transition positions (where the predicted classification changed from one motion type to another) offer additional insights for checking the unique characteristics of the biomechanical (ultrasound) and neuroelectrical (sEMG) signals. To explore the potential characteristics of the two different types of signals, the classification sequences from the two models were post-processed to find the motion transition positions (from one to another motion), which are the closest positions towards the ground truth transition positions. The absolute distances between these two types of positions were then calculated and summarized in the histogram of Figure 8, which shows the relative errors (compared with the ground truth) of the transition positions classified from the model and post-processed to obtain.
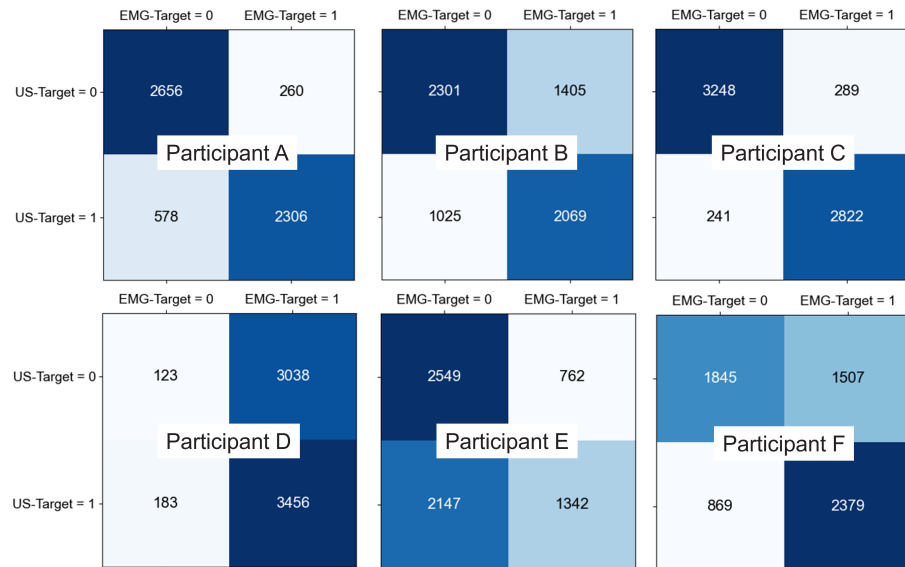
**Figure 7.** The contingency tables compare the full sequence classification only between the ultrasound and sEMG signals, regardless of the ground truth labels. The results of the six participants (**A**–**F**) are arranged in a zigzag pattern from top left to the bottom right. In each table, the row represents the classification of sEMG model (0 means putting down the arm, 1 means lifting up the arm), and the columns indicate the decisions from the ultrasound model. The number in each cell of the table denotes the counts of samples falling into this category (the ultrasound and sEMG had the same or different classification decisions). Note that these tables do not include any comparison with the ground truth labels. Thus, they can visually represent the relationships between the decisions from the two models
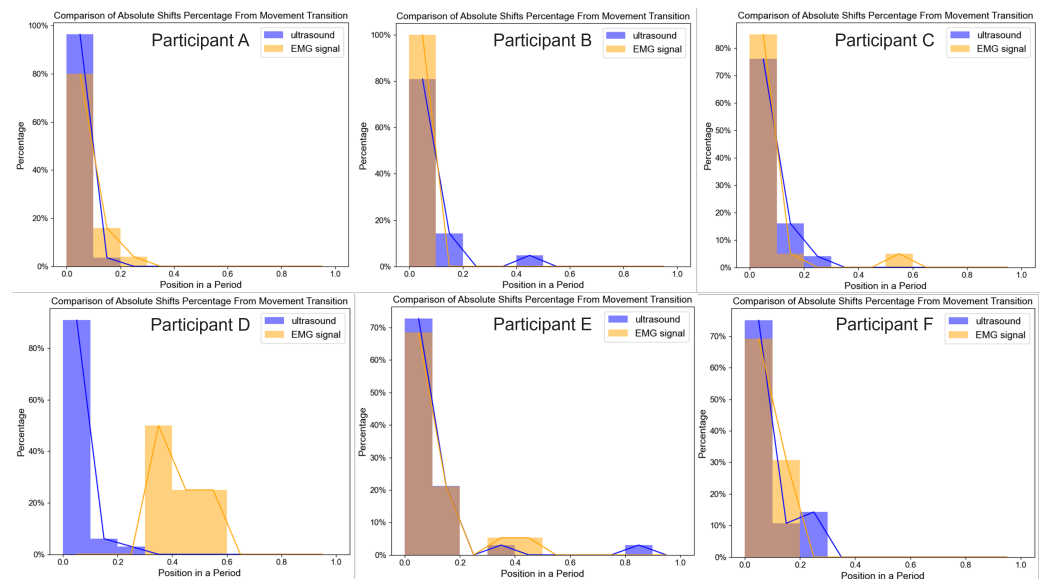


**Figure 8.** The histograms show the distribution of the absolute shift errors between the transition locations of models' classifications (determined by the post-processing from the full sequence classification results) and the transition locations from the ground truth labels, expressed as a percentage of the full motion cycle duration (e.g., 0.2 on the x-axis indicates an error of 20% of the full cycle duration). The results of participants **A** to **F** are arranged from top left to bottom right in a zigzag pattern. The lines connect the peak values of the bars within each distribution slot. The brown color represents the overlapping areas between the results of ultrasound and EMG models. The post-processing steps to obtain the transition locations from the models are described in Section 3.2.

Additionally, if we did not consider the ground truth labels, the transition positions from the two models could also be directly compared, and their distributions across

all motion cycles are summarized in another histogram Figure 9, which highlights the differences in how two different types of models captured the motion transitions from the signals.
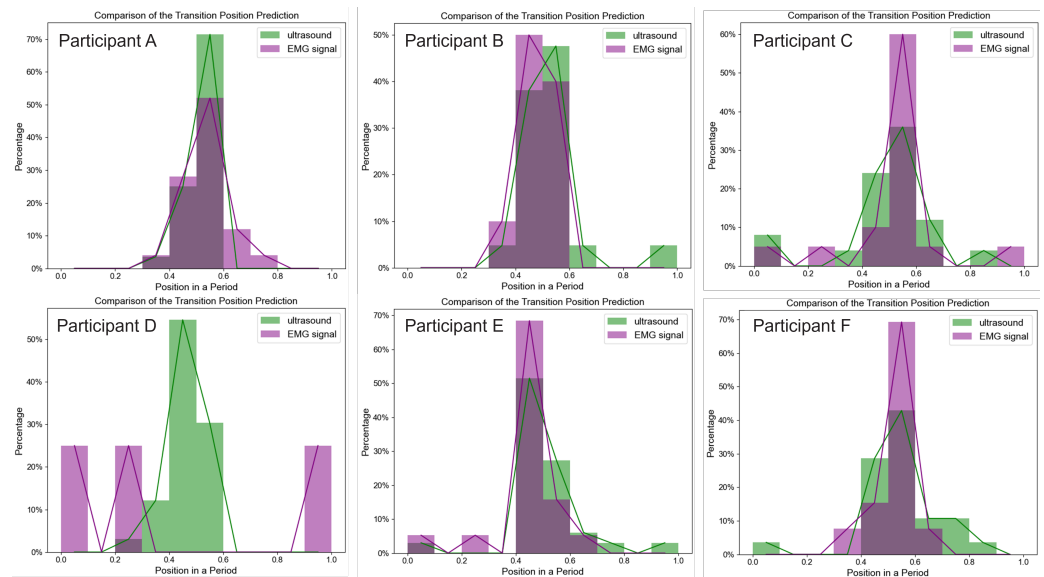


**Figure 9.** The histogram shows the transition locations of the two models' classifications (determined by the post-processing from the full sequence classification results), regardless of ground truth labels, and expressed as a percentage over the single motion cycle (e.g., 0.2 on the x-axis indicates the 20% position of a full cycle duration). The participants **A** to **F** are displayed in a zigzag order from top left to bottom right. The lines connect the peak values of the bars within each distribution slot, illustrating the slot distribution from each participant. The post-processing steps to obtain the transition locations from the models are described in Section 3.2.

## 4. Discussion

Muscle activation and deformation are the key aspects of muscle functionality, but their interplay has not been extensively studied using biological raw signals. Most prior research focused on analyzing these features independently or combining them for specific applications, such as gesture recognition or muscle fatigue analysis. However, the direct correlations between these two muscle properties remain unexplored, leaving a gap in understanding their relationship. This study addressed this gap by investigating how sEMG signals (representing muscle activation) and ultrasound signals (representing muscle deformation) correlate through a motion classification task. By comparing the classification performance of these signals, this research aimed to provide insights into their working mechanism and implications for muscle contraction dynamics.

In the experiment, six participants performed an arm lifting motion, which was categorized into two classes: lifting and putting down the arm. A deep learning model was developed for classifying these motions using the collected signals. The classification results from both types of signals were compared to assess their correlations, facilitating further evaluation of the relationship between muscle activation and deformation. Both models used an attention UNet architecture due to its advantages in the segmentation tasks. As shown in Table 1, the results from both the sequence and transition classifications indicate the correlation between ultrasound and sEMG raw signals. Thus, we used the motion type as the intermediate feature to validate the existence of the relationship between muscle activation and deformation.

For most participants, the analysis results from Table 1 show a significant relationship between ultrasound and sEMG signals, supported by the *p*-values close to 0.00 via the chi-square test. However, participant D was an exception. While a significant correlation

was still observed (*p*-value = 0.0279 < 0.05), the sEMG model's classification performance was less satisfied. As a result, participant D's F1-score for the transition classification was lower compared to that of other participants. The unsatisfied performance may be due to the random arm movements and cycle periods, as well as the special sEMG signal that was more difficult to classify, which will be investigated in a future study.

In Figure 7, the correlations for participants from A to C are evident. The reduced correlations from participant D to F were likely due to the poor classification performance of the sEMG model, as indicated by the low classification accuracy. However, the chi-square significance test still showed *p*-values that were lower than 0.05, showing the existence of correlations between classifications from the ultrasound and sEMG signals. This demonstrated the clear relationship between muscle activation and deformation.

Another perspective of the experimental results was to evaluate how precisely the sEMG and ultrasound models classified the transition types and identified the transition positions. The transition classification task assessed the models' capabilities to capture the patterns of joint angle change within a single period. As shown on the right side of Table 1, the ultrasound model showed good classification performance, due to the clear relationship between muscle deformation and the joint angles [41]. In contrast, the sEMG model exhibited lower accuracy, potentially attributed to the weaker correlation between muscle activation (energy-based variables) and the joint angles (position-based variables). This aspect requires further investigation in future studies. However, even with the difference in accuracy, the Correlation(%) values were close to or even surpassed the sEMG model's classification accuracy. This indicates that, despite the incorrect classifications of ultrasound models, the sEMG model also made the same wrong classification decisions as the ultrasound's, showing the closed relationship between the muscle deformation and activation patterns.

For transition positions analysis, Figure 6 provides qualitative comparisons. We observed that at the same transition positions from the ultrasound model, the predicted transitions from the sEMG model showed some left or right shifts. However, in most motion cycles, these shifts were minimal, indicating that the sEMG model's transitions were closely aligned with those of the ultrasound model, showing the correlation between the transition positions of the two signals.

In addition to Figure 6, Figure 8 directly compares the errors in the transition positions between the two models. From this figure, we observe that, except for participant D, who exhibited a large variance between the ultrasound and sEMG models, the other participants (A to F, excluding D) showed that the distance between the transition positions of the ground truth and the classifications was smaller than 20% of the single motion cycle. This demonstrates a high level of classification agreement between the two models.

Additionally, Figure 9 directly compares the predicted locations of transition between the two models. From this figure, both ultrasound and sEMG models had good classification performances on the transition positions, which were nearly 50% position of the full motion cycle (except for participant D). The sEMG model had slightly earlier prediction than the ultrasound. This may be because the muscle activation has around 100 ms to 200 ms advanced to the actual muscle deformation [14].

Although our method used the motion type as an intermediate to find the relationship between muscle activation and deformation, there were still some limitations in our method. (1) The sEMG signal acquisition process may be influenced by the slight relative movement between electrodes and skin during arm motion, as well as the potential cross-talk between adjacent muscles, such as the biceps brachii and brachialis. However, the influence of these factors could be minimized, as this study focused on the general activation patterns rather than isolating individual muscle signals. Future work could further address the

challenges by using high-density sEMG arrays for measurement [42] or improved electrode designs [43] to enhance the precision and reduce the signal cross-talk issues. (2) Although we directly compared the results of the sEMG model and ultrasound model, we still used the angle joint as the intermediate factor. In future studies, the direct relationship between ultrasound and sEMG signals could be built for better correlation analysis. (3) To measure the direct relationship between ultrasound and sEMG in a fair way, we trained the ultrasound and sEMG models using the same network architecture and the same epoch number, without considering the special signal features or the better classification models for each of them separately. Normally, the sEMG signal is more complex than the A-mode ultrasound signal in both the spacial and temporal domains, so a hierarchical transformer structure considering both domains could be beneficial to extract the motion class information from sEMG signals. However, we still observed that even when the sEMG model performed worse than the ultrasound model, its classification decisions still had a significant relationship (verified from the chi-square test) with the ultrasound, indicating the close relationship between muscle activation and deformation. (4) To show the relationships between the two muscle features, this experiment was only performed using a single type of motion, without exploring on other types of motions. However, as there was no constraint for participants' motion ranges and rhythms, this single motion had diverse muscle activities with a high level of freedom, potentially providing sufficient data to reveal this relationship.

In future research, more analysis could be performed to explore the potential quantitative relationship between these two signals with more types of motions, which can show a clearer relationship between muscle activation and deformation patterns. This study of the correlations between muscle different types of signals can enable more possibilities and potentials for the downstream tasks, such as the study of different muscle contraction dynamics to distinguish the normal and fatigue conditions or the study of the functional relationship of muscles applied in different joints during movement.

## 5. Conclusions

In this paper, we presented a method to identify the direct relationship between muscle deformation and activation, using the original neuromuscular signals. Our experimental results demonstrated the clear correlations between muscle deformation and activation. This research potentially paves the way for further analysis of other predictive features and correlations of muscles, such as force, joint torque, and joint angle. Additionally, it has practical implications and provides insights for downstream applications, including fatigue analysis or muscle disease diagnostics.

**Institutional Review Board Statement:** This human-related experiment had been permitted by the Ethics Committee of Information & Computer Science at the University of Twente (Application No. 240688).

**Informed Consent Statement:** Each participant was notified of the experiment details from the information letter and signed the consent form before the experiments.

**Data Availability Statement:** The measured data was not available due to privacy restrictions, which was described in the consent form signed by the participants.

**Conflicts of Interest:** The authors declare no conflicts of interest.

## Abbreviations

The following abbreviations are used in this manuscript:

| | |
|---|---|
| US | Ultrasound |
| sEMG | Surface Electromyography |
| e.g. | For Example |
| i.e. | That is |
| 3D | 3-dimensions |
| Acc | Accuracy |

## References

1. Preston, D.; Shapiro, B. Basic electromyography: Analysis of motor unit action potentials. In *Electromyography and Neuromuscular Disorders: Clinical-Electrophysiologic Correlations*; Elsevier: Philadelphia, PA, USA, 2005; pp. 215–229.
2. Wakeling, J.M.; Ross, S.A.; Ryan, D.S.; Bolsterlee, B.; Konno, R.; Domínguez, S.; Nigam, N. The energy of muscle contraction. I. Tissue force and deformation during fixed-end contractions. *Front. Physiol.* **2020**, *11*, 813.
3. Taneja, K.; He, X.; Hodgson, J.; Sinha, U.; Sinha, S.; Chen, J. Investigating the Correlation between Force Output, Strains, and Pressure for Active Skeletal Muscle Contractions. *arXiv* **2023**, arXiv:2310.06191v1.
4. Essers, J.; Meijer, K.; Peters, A.; Murgia, A. The effects of facioscapulohumeral dystrophy and dynamic arm support on upper extremity muscle coordination in functional tasks. *Neuromuscul. Disord.* **2023**, *33*, 651–659. https://doi.org/10.1016/j.nmd.2022.11.002.
5. Ma, X.; Zhang, X.; Xu, J. Robotic Leg Prosthesis: A Survey From Dynamic Model to Adaptive Control for Gait Coordination. *IEEE Trans. Neural Syst. Rehabil. Eng.* **2024**, *32*, 607–624. https://doi.org/10.1109/TNSRE.2024.3356561.
6. Slade, P.; Atkeson, C.; Donelan, J.M.; Houdijk, H.; Ingraham, K.A.; Kim, M.; Kong, K.; Poggensee, K.L.; Riener, R.; Steinert, M.; et al. On human-in-the-loop optimization of human–robot interaction. *Nature* **2024**, *633*, 779–788.
7. Nakatani, M.; Takai, Y.; Kanehisa, H. Resistance training leading to repetition failure increases muscle strength and size, but not power-generation capacity in judo athletes. *PLoS ONE* **2024**, *19*, e0307841.
8. Palermi, S.; Massa, B.; Vecchiato, M.; Mazza, F.; De Blasiis, P.; Romano, A.M.; Di Salvatore, M.G.; Della Valle, E.; Tarantino, D.; Ruosi, C.; et al. Indirect structural muscle injuries of lower limb: Rehabilitation and therapeutic exercise. *J. Funct. Morphol. Kinesiol.* **2021**, *6*, 75.
9. Tweedell, A.J.; Tenan, M.S.; Haynes, C.A. Differences in muscle contraction onset as determined by ultrasound and electromyography. *Muscle Nerve* **2019**, *59*, 494–500.
10. Yang, X.; Yan, J.; Liu, H. Comparative Analysis of Wearable A-Mode Ultrasound and sEMG for Muscle-Computer Interface. *IEEE Trans. Biomed. Eng.* **2020**, *67*, 2434–2442. https://doi.org/10.1109/TBME.2019.2962499.
11. Zeng, J.; Zhou, Y.; Yang, Y.; Wang, J.; Liu, H. Feature Fusion of sEMG and Ultrasound Signals in Hand Gesture Recognition. In Proceedings of the 2020 IEEE International Conference on Systems, Man, and Cybernetics (SMC), Toronto, ON, Canada, 11–14 October 2020; pp. 3911–3916. https://doi.org/10.1109/SMC42975.2020.9282818.
12. Zeng, J.; Zhou, Y.; Yang, Y.; Xu, Z.; Zhang, H.; Liu, H. Robustness of combined sEMG and ultrasound modalities against muscle fatigue in force estimation. In Proceedings of the Intelligent Robotics and Applications: 14th International Conference, ICIRA 2021, Yantai, China, 22–25 October 2021; Proceedings, Part III 14; Springer: Berlin/Heidelberg, Germany, 2021; pp. 213–221.
13. Botter, A.; Carbonaro, M.; Vieira, T.M.; Hodson-Tole, E. Identification of muscle fasciculations from surface EMG: Comparison with ultrasound-based detection. In Proceedings of the 2019 41st Annual International Conference of the IEEE Engineering in Medicine and Biology Society (EMBC), Berlin, Germany, 23–27 July 2019; pp. 5117–5120. https://doi.org/10.1109/EMBC.2019.8857873.
14. Song, T.; Yan, Z.; Guo, S.; Li, Y.; Li, X.; Xi, F. Review of sEMG for robot control: Techniques and applications. *Appl. Sci.* **2023**, *13*, 9546.
15. Yang, X.; Chen, Z.; Hettiarachchi, N.; Yan, J.; Liu, H. A wearable ultrasound system for sensing muscular morphological deformations. *IEEE Trans. Syst. Man, Cybern. Syst.* **2019**, *51*, 3370–3379.
16. Niu, K.; Homminga, J.; Sluiter, V.I.; Sprengers, A.; Verdonschot, N. Feasibility of A-mode ultrasound based intraoperative registration in computer-aided orthopedic surgery: A simulation and experimental study. *PLoS ONE* **2018**, *13*, e0199136.
17. Barsotti, G.; Citi, S.; Brovelli, M.; Mussi, E.; Luchetti, E.; Carlucci, F.; Sgorbini, M. Equine ocular ultrasonography: Evaluation of some biometric measurements. *Ippologia* **2010**, *21*, 39–43.
18. Hamidzada, W.A.; Osuobeni, E.P. Agreement between A-mode and B-mode ultrasonography in the measurement of ocular distances. *Vet. Radiol. Ultrasound* **1999**, *40*, 502–507.

19. Schouten, M.; van de Maat, P.; Nizamis, K.; Krijnen, G. Evaluating 3D printed sEMG electrodes with silver ink traces using in-situ impedance measurements. In Proceedings of the 2022 IEEE Sensors, Dallas, TX, USA, 30 October–2 November 2022; pp. 1–4.

20. Pocock, G.; Richards, C.D.; Richards, D.A. *Human Physiology*; Oxford University Press: Cary, NC, USA, 2013.

21. Niu, K.; Homminga, J.; Sluiter, V.; Sprengers, A.; Verdonschot, N. Measuring relative positions and orientations of the tibia with respect to the femur using one-channel 3D-tracked A-mode ultrasound tracking system: A cadaveric study. *Med. Eng. Phys.* **2018**, *57*, 61–68.

22. Niu, K.; Sluiter, V.; Homminga, J.; Sprengers, A.; Verdonschot, N. A novel ultrasound-based lower extremity motion tracking system. In *Intelligent Orthopaedics: Artificial Intelligence and Smart Image-Guided Technology for Orthopaedics*; Springer: Berlin/Heidelberg, Germany, 2018; pp. 131–142.

23. Niu, K.; Anijs, T.; Sluiter, V.; Homminga, J.; Sprengers, A.; Marra, M.A.; Verdonschot, N. In situ comparison of A-mode ultrasound tracking system and skin-mounted markers for measuring kinematics of the lower extremity. *J. Biomech.* **2018**, *72*, 134–143.

24. Niu, K.; Sluiter, V.; Lan, B.; Homminga, J.; Sprengers, A.; Verdonschot, N. A Method to Track 3D Knee Kinematics by Multi-Channel 3D-Tracked A-Mode Ultrasound. *Sensors* **2024**, *24*, 2439.

25. Cao, Z.; Simon, T.; Wei, S.E.; Sheikh, Y. Realtime multi-person 2d pose estimation using part affinity fields. In Proceedings of the IEEE Conference on Computer Vision and Pattern Recognition (CVPR), Honolulu, HI, USA, 21–26 July 2017; pp. 7291–7299.

26. Lee, P.; Chen, T.B.; Lin, H.Y.; Yeh, L.R.; Liu, C.H.; Chen, Y.L. Integrating OpenPose and SVM for Quantitative Postural Analysis in Young Adults: A Temporal-Spatial Approach. *Bioengineering* **2024**, *11*, 548.

27. Yazdani, A.; Novin, R.S.; Merryweather, A.; Hermans, T. Occlusion-Robust Multi-Sensory Posture Estimation in Physical Human-Robot Interaction. *arXiv* **2022**, arXiv:2208.06494.

28. Li, Z.; Yeow, R.C.H. PoseAction: Action Recognition for Patients in the Ward using Deep Learning Approaches. *arXiv* **2023**, arXiv:2310.03288.

29. Favre, J.; Aissaoui, R.; Jolles, B.M.; de Guise, J.A.; Aminian, K. Functional calibration procedure for 3D knee joint angle description using inertial sensors. *J. Biomech.* **2009**, *42*, 2330–2335.

30. Di Raimondo, G.; Vanwanseele, B.; Van der Have, A.; Emmerzaal, J.; Willems, M.; Killen, B.A.; Jonkers, I. Inertial sensor-to-segment calibration for accurate 3d joint angle calculation for use in OpenSim. *Sensors* **2022**, *22*, 3259.

31. Seel, T.; Raisch, J.; Schauer, T. IMU-based joint angle measurement for gait analysis. *Sensors* **2014**, *14*, 6891–6909.

32. Lan, B.; Abayazid, M.; Verdonschot, N.; Stramigioli, S.; Niu, K. SIRC-UNet: Improving Bone Tracking Precision of A-mode Ultrasound by Decoding Hierarchical Resolution Features. *IEEE Sens. J.* **2024**, *24*, 38174–38184.

33. Memar Ardestani, M.; Yan, H. Noise reduction in human motion-captured signals for computer animation based on B-spline filtering. *Sensors* **2022**, *22*, 4629.

34. Liu, G.; McMillan, L. Estimation of missing markers in human motion capture. *Vis. Comput.* **2006**, *22*, 721–728.

35. Tits, M.; Tilmanne, J.; Dutoit, T. Robust and automatic motion-capture data recovery using soft skeleton constraints and model averaging. *PLoS ONE* **2018**, *13*, e0199744.

36. Lan, B.; Stramigioli, S.; Niu, K. Anatomical Region Recognition and Real-time Bone Tracking Methods by Dynamically Decoding A-Mode Ultrasound Signals. *arXiv* **2024**, arXiv:2405.19542.

37. Lan, B.; Abayazid, M.; Verdonschot, N.; Stramigioli, S.; Niu, K. Deep Learning based acoustic measurement approach for robotic applications on orthopedics. *arXiv* **2024**, arXiv:2403.05879.

38. Clevert, D.A. Fast and accurate deep network learning by exponential linear units (elus). *arXiv* **2015**, arXiv:1511.07289.

39. Kingma, D.P. Adam: A method for stochastic optimization. *arXiv* **2014**, arXiv:1412.6980.

40. Barceló, J.A. Chi-square analysis. In *The Encyclopedia of Archaeological Sciences*; Wiley: Hoboken, NJ, USA, 2018; pp. 1–5.

41. Sagawa, R.; Ayusawa, K.; Yoshiyasu, Y.; Murai, A. Predicting muscle activity and joint angle from skin shape. In Proceedings of European Conference on Computer Vision (ECCV) Workshops, Munich, Germany, 8–14 September 2018.

42. Campanini, I.; Merlo, A.; Disselhorst-Klug, C.; Mesin, L.; Muceli, S.; Merletti, R. Fundamental concepts of bipolar and high-Density surface EMG understanding and teaching for clinical, occupational, and sport applications: Origin, detection, and main errors. *Sensors* **2022**, *22*, 4150.

43. Varghese, R.J.; Pizzi, M.; Kundu, A.; Grison, A.; Burdet, E.; Farina, D. Design, Fabrication and Evaluation of a Stretchable High-Density Electromyography Array. *Sensors* **2024**, *24*, 1810.